Multilayer perceptron model vs charge comparison method for neutron/gamma discrimination in plastic scintillator according to sampling frequency and energy radiation

Ali Hachem, Yoann Moline, Gwenolé Corre, Jérôme Gauthier, Frédérick Carrel

Multilayer Perceptron Model vs Charge Comparison Method for Neutron/Gamma Discrimination in Plastic Scintillator According to Sampling Frequency and Energy Radiation

A. Hachem, Y. Moline, G. Corre, J. Gauthier and F. Carrel

***Abstract*—Pulse shape discrimination algorithms have been commonly implemented on embedded systems to discriminate neutron/gamma radiations detected by organic scintillators in several applications. These algorithms have a number of limitations, especially when used with plastic scintillators, which have low intrinsic discriminating ability. Machine learning (ML) models have recently been explored as a way to improve discriminating performance. Most of these methods are proposed for liquid and stilbene scintillators and do not address the integrated implementation. Reducing the sampling frequency of a discrimination system helps to minimize the size and cost of the embedded implementation. The purpose of this study is to explore whether the use of ML tools, compared to the Tail-to-Total integral ratio (TTT_{ratio}) algorithm, can lead to a reduction in the minimum required sampling frequency in EJ276 plastic scintillator, as well as an enhancement in the classification performance. The results obtained highlight the superior performance of the ML model.**

***Index Terms*—EJ276, Neutron Gamma Discrimination, Plastic Scintillator, Organic Scintillators, Machine Learning, MultiLayer Perceptron Model, sampling frequency, radiation energy**

I. Introduction

Organic scintillators have been developed to detect neutrons and gamma-rays and are used in many applications such as homeland security. Tail to total integral ratio algorithm (TTT_{ratio}), which is also called Charge Comparison Method (CCM), has been widely used to discriminate the detected events [1]–[6]. This algorithm relies on the shape difference of the signals to classify them. The interaction of a neutron results in a longer signal than that generated by a gamma-ray (Fig. 1) [7]. In liquid and stilbene scintillators, the difference between the two created signals is more significant than the plastic counterpart. Consequently, this discrimination approach perform better with these types of detectors [4], [8], [9]. In contrast, plastic scintillators have several advantages. They can be shaped more easily, manufactured in a larger volume, have a lower cost, and are non-toxic [10].

The power consumption of an embedded discrimination system is influenced by its sampling frequency. By decreasing the frequency of digital pulse processing, it becomes possible to integrate an approach with less cost and size. The objective of this work is to examine whether employing ML tools can decrease the minimum sampling frequency needed for distinguishing between neutrons and gamma-rays in EJ276 plastic scintillators, while simultaneously improving the classification accuracy. First, we compared the discrimination ability as a function of radiation energy to show that the ML approach can improve the discrimination, especially at low energy. Then, we studied how much the sample rate may be decreased for both approaches without significantly impairing the discriminating ability. Raw signals were produced and labeled using the labeling strategy proposed in [11] to train the model and compare both approaches. It is important to note that this process can be applied to any organic or inorganic scintillator to assess whether ML tools can enhance discrimination performance or reduce the necessary sampling frequency.

Section II introduces TTT_{ratio} algorithm and review the most recent developments in ML methods for neutron/gamma discrimination. The preparation of the training and validation datasets for this study using the radioactivity sources ^{252}Cf and ^{60}Co is then described in section III. Section IV provides a brief explanation of the energy calibration used in the implemented acquisition chain. In section V, the study concludes by presenting the results of training a Multi Layer Perceptron Neural Network (MLP) model on the provided datasets for various energy ranges at various sampling rates. The comparison with the TTT_{ratio} method emphasizes the MLP model's superior performance.

To the best of our knowledge, this is the first work that compares the discrimination performance of a ML model and the TTT_{ratio} algorithm in a plastic scintillator, for different radiation energy ranges, at different sampling frequencies.

II. Neutron Gamma Discrimination Approach

A. Tail-to-Total Integral Ratio

TTT_{ratio} algorithm is based on the decay time difference between neutron and gamma-ray interactions to differentiate them (Fig. 1). It computes the ratio between the tail and total integral of the signals, as shown in equation 1.

$$TTT_{ratio} = \frac{Q_{tail}}{Q_{total}} \tag{1}$$

where $Q_{tail} = \int_{t_{short}}^{t_{long}} f(t)$ and $Q_{total} = \int_{0}^{t_{long}} f(t)$
t_{long} and t_{short} are tuned to optimize the discrimination performance.

A. Hachem, Y. Moline, G. Corre J. Gauthier and F. Carrel are with Paris-Saclay University (Physic Department) and CEA-LIST: Laboratory for Integration of Systems and Technology, 91191 Gif-sur-Yvette, France (e-mail: ali.hachem@cea.fr)

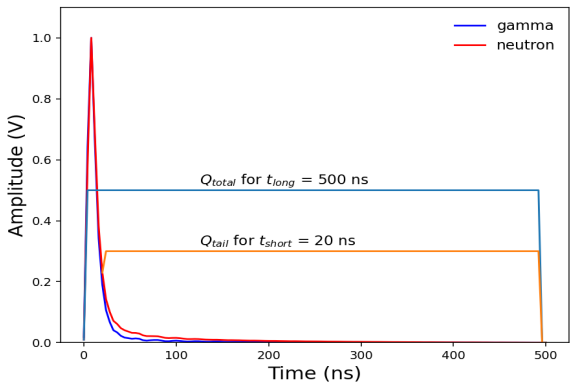

Fig. 1. Average of neutron and gamma-ray signals detected by EJ276 plastic scintillator at 250 MHz. Use of a ^{252}Cf neutron source. The number of neutron and gamma signals is respectively 40600 and 66800. Min-max normalization is applied on the average signals.

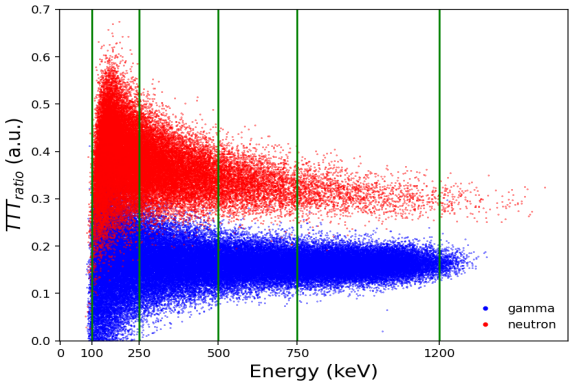

Fig. 2. Bi-parametric histogram of TTT_{ratio} according to the total energy integral obtained from the labeled datasets at 250 MHz. The green lines indicate the energy intervals that have been chosen to compare the results.

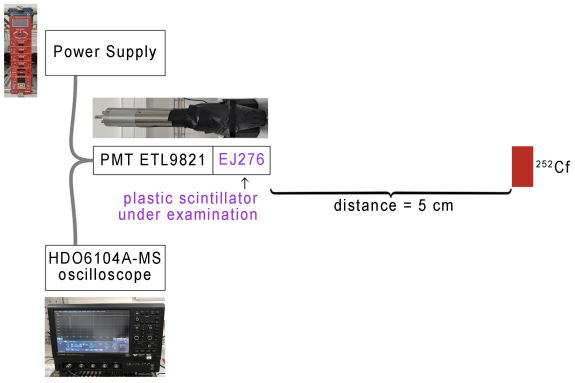

Fig. 3. Implemented acquisition chain.

B. ML Tools

ML techniques have been explored to improve discrimination performance in liquid and stilbene scintillators [12]–[17]. The authors of [12] propose a non-negative matrix factorization to discriminate neutrons and gamma-rays with stilbene scintillator. Another study proposes a Gaussian Mixture model with EJ309 liquid scintillator [13]. In [14] and [15], the authors implement an Artificial Neutral network and Support Vector Machine to achieve the discrimination in stilbene and liquid scintillator, respectively. Another ML model is proposed in [18] to classify radiations detected by the EJ299-33 plastic scintillator. While the discrimination performance is improved in the three previous studies, the ML models were trained on datasets labeled by TTT_{ratio} discrimination algorithm. The accuracy of the labeling by this algorithm is decreased when dealing with relatively low energy radiations due to a significant overlap between the TTT_{ratio} distributions of neutrons and gamma-rays (Fig. 2). Choosing one TTT_{ratio} threshold to classify the signals results to a significant number of mislabeled samples. Furthermore, if an energy radiation threshold is selected, above which neutrons and gamma-rays can be distinguished from each other, then using machine learning would become unnecessary. This is because simpler methods can be used to separate the two types of radiation.

III. Data Preparation

The acquisition chain of this study is composed of an EJ276 plastic scintillator coupled to a PMTETL9821 photomultiplier powered at 1700 V. The latter is connected to a HDO6104A-MS oscilloscope (12 bits). The radiation source is placed a few centimeters away from the scintillator (Fig. 3).

In our previous work, we showed that the minimal sampling rate needed to execute the TTT_{ratio} algorithm with this acquisition chain without a significant performance loss is 250 MHz [19]. Therefore, we created two datasets at sampling rates of 125 MHz and 250 MHz. As a consequence, we can examine whether utilizing ML tools instead of the TTT_{ratio} method, the minimum sample rate required to achieve neutron/gamma discrimination with the EJ276 scintillator can be reduced. This reduction helps to obtain an embedded discrimination system with less power consumption and complexity.

It should be noted that preparing a dataset at lower sampling frequency (less than 125 MHz) results in a loss of signal shape and amplitude, which includes the necessary information to carry out the discrimination. Thus, the classification performance deteriorates sharply at this low level of sampling rate for the implemented acquisition chain of this study. This is expected since the average rise time and the first decay time component of the scintillator are 6 ns and 13 ns respectively, and the maximum frequency component obtained by the Fast Fourier Transform of the recorded signals is 100 MHz [19].

The raw signals at 250 MHz were first prepared. Neutron samples were obtained through our labeling pipeline proposed in [11], using ^{252}Cf source. The first step in the process was acquiring the signals via an implemented time of flight (ToF) setup (Fig.4). Acquired and labeled signals by ToF often contain mislabeled samples, which have various origins, such as the overlap between the gamma and neutron arrival time distributions and natural background radiations. The next step involved identifying and removing pile-up events, as experimental results showed that these events are relatively prevalent in the collected datasets. The remaining signals were then processed to decrease the number of background events and labeled based on ToF information. The final step of the pipeline is reducing the percentage of mislabeled

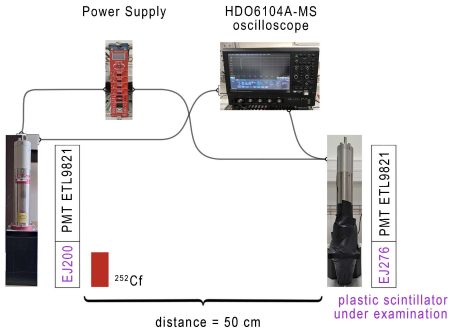

Fig. 4. Implemented ToF experiment.

samples present in the obtained datasets using a TTT_{ratio} discrimination algorithm. A method is introduced to select a convenient TTT_{ratio} that is used to remove mislabeled neutron samples.

Gamma-ray dataset was directly acquired from ^{60}Co. The t_{short} and t_{long} parameters were tuned using [20], with the resulting optimum values being 20 ns and 500 ns, respectively. These settings were used in the labeling process and to obtain the results of section V. The triggering threshold, the voltage peak to peak, and the acquisition window are all set to 15 mV, 800 mV and 1 μs, respectively. The length of each signal is 500 ns from its starting point (10% of the maximum).

Concerning the preparation of labeled datasets at 125 MHz, the proposed labeling strategy in [11] cannot be used. The latter depends on TTT_{ratio} algorithm, which with the present acquisition chain is unable to differentiate the signals at this frequency level [19]. One solution could be to use the dataset prepared at 250 MHz, then downsampling the recorded signals.

Downsampling consists in reducing the sampling rate (f_s) of a signal. The rate reduction by a factor *N* can be done by the following two steps [21]:

1) Reduce the high frequency components of the signals with a low pass filter to avoid potential aliasing. The cutoff frequency of the filter is equal to $f_s/(2 * N)$.
2) Decimate the filtered signal by *N*. In other words, keep only every N^{th} sample.

In the presented case, neutron dataset is prepared at 125 MHz using a Butterworth digital Finite Impulse Response filter [22]. The window of the implemented filter is *Kaiser* [23] with β and length equal to 6 and $200 * f_s$, respectively. This filter's frequency response in the pass band ([0 - 62.5 MHz]) needed to produce the downsampled dataset is flat, as shown in Fig. 5.

It should be noted that downsampled signals, though realistic, are still somewhat different to signals acquired directly at 125 MHz sampling rate in which some of the information required to perform the discrimination might be lost while these information in the downsampled signal may be preserved. Nevertheless, obtaining a pure neutron dataset at this relatively low sampling frequency is not possible for us at the time this article was written and using downsampled version is a reasonable approach to develop our methodology.

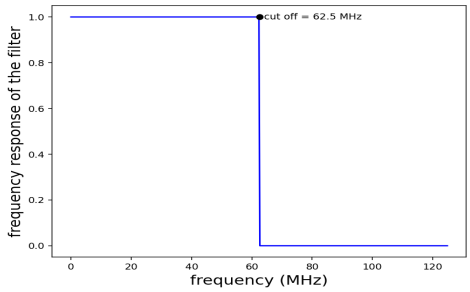

Fig. 5. Frequency response of the Butterworth digital Finite Impulse Response filter used to obtain the downsampled dataset (f_s = 125 MHz).

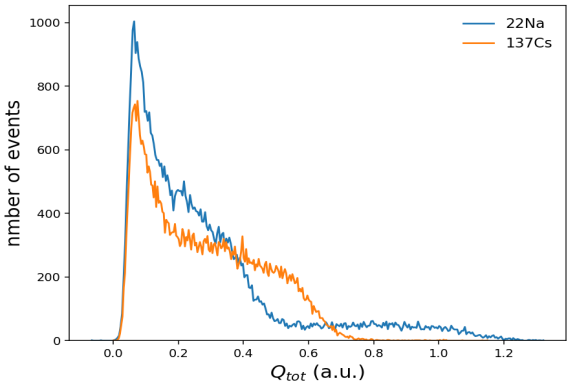

Fig. 6. Examples of the spectrum obtained from ^{137}Cs and ^{22}Na sources with a plastic scintillator and a PMT.

IV. Energy Calibration

The pulses distribution as a function of the total integral (Q_{total}) was used to calibrate the energy of the implemented acquisition chain (examples of ^{137}Cs and ^{22}Na shown in Fig. 6). This calibration process was carried out according to the procedure proposed in [24]. A comparison was made between the measured and simulated spectrum, taking into account the degradation of energy resolution represented by the Gaussian energy broadening (GEB) function. The simulation was performed using the Monte Carlo N-Particle code (MCNP6.2 [25]), where the values of parameters *a, b,* and *c* were 0.02, 0.1, and -0.2953, respectively. Thereafter, we used the obtained Compton maximum energies of ^{137}Cs, and ^{22}Na, and the photopeaks of ^{241}Am (Table I). A linear energy response function was then applied for the calibration. Results presented in section V were obtained for an energy radiation higher than 100 keV, as shown in Fig. 2.

Thanks to this energy calibration, the comparison between the trained ML model and the TTT_{ratio} algorithm can be performed according to the energy variation to evaluate its impact on the discrimination performance.

V. ML Model

A. Implementation

The number of neutron and gamma-ray signals prepared at 250 MHz are 40600 and 66800, respectively. These datasets are separated into 80% for the training and 20 % for the validation. The optimizer algorithm is Adam, and the loss function is

TABLE I
THE CORRESPONDING Q_{tot} FOR DIFFERENT ENERGY LEVELS BASED ON THE RESULT OBTAINED BY THE SIMULATION FOR THE ENERGY CALIBRATION.

source	energy (keV)	Q_{tot} (a.u.)
^{22}Na	323	0.24
^{22}Na	1020	1.02
^{137}Cs	456	0.5
^{241}Am	60	0.052

TABLE II
CLASSIFICATION REPORT OF THE VALIDATION DATA ACQUIRED AT SAMPLING RATE EQUAL TO 250 MHZ. ACCURACY IS EQUAL TO 98%.

class	precision	recall	f1-score
gamma-ray	98%	98%	98%
neutron	97%	97%	97%

binary cross-entropy. The number of epochs, waiting epochs, and batch size are assigned to 200, 10, and 16 respectively. ReLU and Sigmoid are respectively the activation functions of the hidden and last layers. The Keras framework and Scikit-learn package are used for the implementation.

The inference time of any proposed ML solution is critical for time constrained applications. It can be reduced by optimizing the model size, which can be done by tuning the number of layers and the number of neurons in each layer without significant loss of discrimination performance. The resulting model of the adjustment is one with two hidden layers of 32 neurons each. The input layer has n neurons, which is the number of points encoding a signal. The output layer is one neuron represents the probability that a signal will be a neutron or gamma. If the output is more than 0.5, the radiation is considered to be a neutron, otherwise, it is a gamma. In other words, the standard categorization threshold is 0.5. For the TTT_{ratio} algorithm, a chosen value of TTT_{ratio} that depends on the acquisition chain is used as a classification threshold.

Receiver Operating Characteristic (ROC) curve is a graph that illustrates the diagnostic ability of a binary classifier system as its discrimination threshold is varied. It is created by plotting the True Positive Rate (TPR) versus the False Positive Rate (FPR) at various threshold settings. By plotting this curve, the comparison between the proposed MLP model and the TTT_{ratio} method will be performed.

B. Experimental Results

The implemented MLP model was trained and tested using datasets prepared at a sampling rate of 250 MHz. The classification report of the validation dataset is shown in Table II). The obtained TPR is 97%. Accordingly, 30 samples out of every 1000 neutrons will be categorized as gamma-rays. Furthermore, the model raises 20 false alarms for every 1000 gamma signals it classifies. The FPR is thus equivalent to 2%.

Fig. 7 displays the ROC curves obtained by the trained model and TTT_{ratio} algorithm at 250 MHz for various radiation energy ranges. The Q_{tot} for each energy level obtained according to the results of the energy calibration is shown in Table III. It is clear that the discrimination performance of both

TABLE III
THE CORRESPONDING Q_{tot} FOR DIFFERENT ENERGY LEVELS BASED ON THE RESULT OBTAINED BY THE ENERGY CALIBRATION. COLUMN THREE REPRESENTS THE PERCENTAGE OF EACH ENERGY RANGE IN THE VALIDATION DATASET (f_s = 250 MHZ).

energy (keV)	Q_{tot} (a.u.)	percentage
$[100, 250]$	$[0.06, 0.22]$	38%
$[250, 500]$	$[0.22, 0.49]$	27%
$[500, 750]$	$[0.49, 0.75]$	15%
$[750, 1200]$	$[0.75, 1.3]$	20%

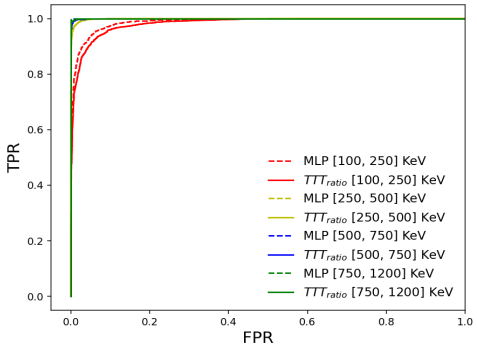

(a) ROC curve

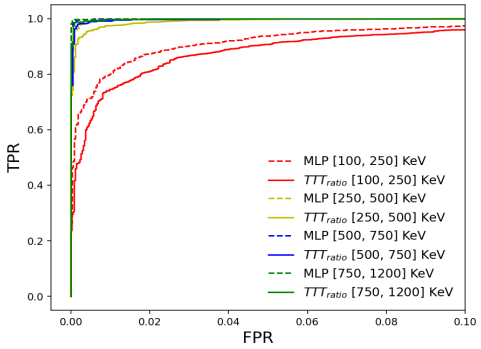

(b) Zoom in ROC curve

Fig. 7. ROC curves obtained by MLP model and TTT_{ratio} discrimination algorithm on validation data, for different energy ranges, f_s = 250 MHz. The ROC curves for the energy ranges [500 keV, 750 keV] and [750 keV, 1.2 MeV] are superimposed. The discrimination threshold that provides a certain level of FPR for the entire dataset is different from the thresholds that provide the same level of FPR for different subsets of the data. Thus, for the same level of FPR, the average TPR is not equal to the TPR of the entire dataset. The latter is equal to the former if the same discrimination threshold is used.

approaches degrades as the energy levels decrease. The trained model nonetheless maintains its superiority, particularly with low energy radiations. This is seen from the sharp contrast between the ROC curves for the [100 keV, 250 keV] energy range. Moreover, the model's area under the ROC curve (AUC) for energies greater than 500 keV is exactly 100%, in contrast to the TTT_{ratio} method (99.9%), as shown in Fig. 7.

Thereafter, we prepared training datasets at 125 MHz sampling rate. Then, we created a testing dataset to assess the trained model using a dataset directly obtained at this sampling frequency without the downsampling step. The latter consists of downsampled neutron samples from the validation data and 15000 signals directly acquired at the required sampling rate using the gamma-ray source ^{60}Co.

The same MLP model is trained on the prepared training

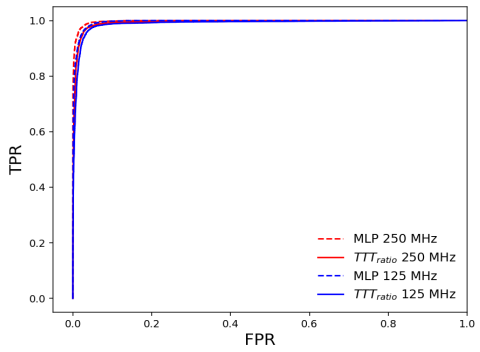

(a) ROC curve

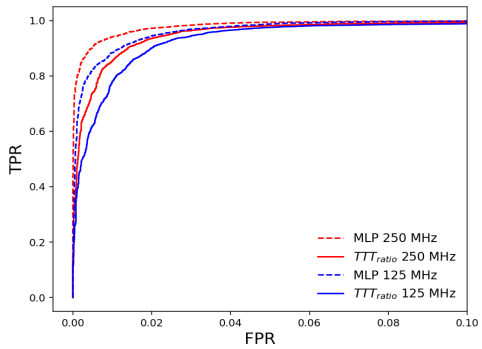

(b) Zoom in ROC curve

Fig. 8. ROC curves obtained by MLP model and TTT_{ratio} discrimination algorithm on testing data at different sampling rates.

TABLE IV
OBTAINED ACCURACY, TPR AND FPR WITH MLP ON VALIDATION (TESTING) DATASET AT 250 MHZ (125 MHZ).

		FPR = 2%	
f_s	accuracy	TPR	TPR for TTT_{ratio}
250 MHz	98%	97%	94%
125 MHz	97%	94%	90%

dataset. The obtained results on the testing data following the training in Table IV indicates that the model performance is proportional to the sampling frequency. Moreover, Fig.8 illustrates how the model outperforms the TTT_{ratio} method at 125 MHz and 250 MHz. For instance, the former's TPR is 94% when the FPR is equal to 2%. The latter, in comparison, offers TPRs of 90% and 93%, respectively, for the same FPR level, at both sampling rates (Table IV).

In summary, TTT_{ratio} method is a better option for embedded implementing since its computing complexity is relatively lower than that of a trained MLP model. The latter involves 5088 multiplications (126*32+32*32+32) and one division, whereas the TTT_{ratio} method requires only one division operation. However, the previous results shows that this algorithm performs worse than the MLP model for various energy ranges at low sampling rates. Moreover, the integration of a trained MLP model on an embedded device with relatively low inference time has recently become feasible [26], [27].

VI. CONCLUSION

In this study, we compared the discrimination performance on neutron/gamma signals recorded using an EJ276 plastic scintillator between a trained MLP model and the TTT_{ratio} algorithm. The ability to discriminate was first compared according to the variation of the energy radiation. In the presented case, the performance of both methods decreases with the energy of the incident radiation. Nevertheless, the trained model outperforms the TTT_{ratio} algorithm, especially for low energy radiations ([100 keV, 250 keV]). Then, the performance of discrimination was examined according to the sampling frequency. The trained model outperforms the discriminating algorithm in terms of its ability to distinguish the radiations at lower sampling rates.

In conclusion, ML tools are a promising solution to perform neutron gamma discrimination in plastic scintillators for embedded applications. They can help to reduce the architecture size, power and complexity of an online discrimination system. Nevertheless, altering any element or parameter in the acquisition chain has a significant influence on the output signal's form. A current limitation of our approach is how sensitively the trained model responds to this adjustment. The process of preparing the datasets and training the model should be repeated for any modification in the acquisition chain. Regarding future developments, we will focus our efforts on the robustness of the model, or its ability to adapt to a new dataset obtained through a different acquisition chain without having to go through the learning process again. Another development is the comparison between the implementation of MLP, TTT_{ratio}, and 1D Convolution Neural Network on an FPGA. The comparison considers different factors such as quantization, resource consumption, and execution time. The ultimate aim is to ensure that predictions are made within the signal length duration respecting the resources constraint.

REFERENCES

[1] J. Adams and G. White, "A versatile pulse shape discriminator for charged particle separation and its application to fast neutron time-of-flight spectroscopy," *Nuclear Instruments and Methods*, vol. 156, no. 3, pp. 459–476, 1978.

[2] O. McCormack, L. Giacomelli, G. Croci, A. Muraro, G. Gorini, G. Grosso, R. Pasqualotto, E. P. Cippo, M. Rebai, D. Rigamonti *et al.*, "Characterization and operational stability of ej276 plastic scintillator-based detector for neutron spectroscopy," *Journal of Instrumentation*, vol. 16, no. 10, p. P10002, 2021.

[3] A. Tomanin, J. Paepen, P. Schillebeeckx, R. Wynants, R. Nolte, and A. Lavietes, "Characterization of a cubic ej-309 liquid scintillator detector," *Nuclear Instruments and Methods in Physics Research Section A: Accelerators, Spectrometers, Detectors and Associated Equipment*, vol. 756, pp. 45–54, 2014.

[4] M. Grodzicka-Kobylka, T. Szczesniak, M. Moszyński, K. Brylew, L. Swiderski, J. Valiente-Dobón, P. Schotanus, K. Grodzicki, and H. Trzaskowska, "Fast neutron and gamma ray pulse shape discrimination in EJ-276 and EJ-276G plastic scintillators," *Journal of Instrumentation*, vol. 15, no. 03, p. P03030, 2020.

[5] N. Zaitseva, A. Glenn, A. Mabe, M. Carman, C. Hurlbut, J. Inman, and S. Payne, "Recent developments in plastic scintillators with pulse shape discrimination," *Nuclear Instruments and Methods in Physics Research Section A: Accelerators, Spectrometers, Detectors and Associated Equipment*, vol. 889, pp. 97–104, 2018.

[6] E. Ryabeva, I. Urupa, E. Lupar, V. Kadilin, A. Skotnikova, Y. Kokorev, and R. Ibragimov, "Calibration of ej-276 plastic scintillator for neutron–gamma pulse shape discrimination experiments," *Nuclear Instruments and Methods in Physics Research Section A: Accelerators, Spectrometers, Detectors and Associated Equipment*, vol. 1010, p. 165495, 2021.

[7] F. Brooks, "Development of organic scintillators," *Nuclear Instruments and Methods*, vol. 162, no. 1-3, pp. 477–505, 1979.

[8] T. Laplace *et al.*, "Comparative scintillation performance of EJ-309, EJ-276, and a novel organic glass," *Journal of Instrumentation*, vol. 15, no. 11, p. P11020, 2020.
[9] F. Ferrulli, N. Dinar, L. G. Manzano, M. Lablme, and M. Silari, "Characterisation of stilbene and EJ-276 scintillators coupled with a large area sipm array for a fast neutron dose rate detector," *Nuclear Instruments and Methods in Physics Research Section A: Accelerators, Spectrometers, Detectors and Associated Equipment*, p. 165566, 2021.
[10] G. F. Knoll, *Radiation detection and measurement*. John Wiley & Sons, 2010.
[11] A. Hachem, Y. Moline, G. Corre, B. Ouni, M. Trocme, A. Elayeb, and F. Carrel, "Labeling strategy to improve neutron/gamma discrimination with organic scintillator," *Nuclear Engineering and Technology*, 2023. [Online]. Available: https://www.sciencedirect.com/science/article/pii/S173857332300339X
[12] H. Arahmane, E.-M. Hamzaoui, and R. Moursli, "Improving neutron-gamma discrimination with stilbene organic scintillation detector using blind nonnegative matrix and tensor factorization methods," *Journal of Spectroscopy*, vol. 2019, pp. 1–9, 05 2019.
[13] L. M. Simms, B. Blair, J. Ruz, R. Wurtz, A. D. Kaplan, and A. Glenn, "Pulse discrimination with a gaussian mixture model on an FPGA," *Nuclear Instruments and Methods in Physics Research Section A: Accelerators, Spectrometers, Detectors and Associated Equipment*, vol. 900, pp. 1–7, 2018.
[14] C. Fu, A. Di Fulvio, S. Clarke, D. Wentzloff, S. Pozzi, and H. Kim, "Artificial neural network algorithms for pulse shape discrimination and recovery of piled-up pulses in organic scintillators," *Annals of Nuclear Energy*, vol. 120, pp. 410–421, 2018.
[15] X. Yu, J. Zhu, S. Lin, L. Wang, H. Xing, C. Zhang, Y. Xia, S. Liu, Q. Yue, W. Wei, Q. Du, and C. Tang, "Neutron–gamma discrimination based on the support vector machine method," *Nuclear Instruments and Methods in Physics Research Section A: Accelerators, Spectrometers, Detectors and Associated Equipment*, vol. 777, pp. 80–84, 2015. [Online]. Available: https://www.sciencedirect.com/science/article/pii/S0168900214015551
[16] A. D. Kaplan, B. Blair, C. Chen, A. Glenn, J. Ruz, and R. Wurtz, "A neutron-gamma pulse shape discrimination method based on pure and mixed sources," *Nuclear Instruments and Methods in Physics Research Section A: Accelerators, Spectrometers, Detectors and Associated Equipment*, vol. 919, pp. 36–41, 2019.
[17] G. Liu, M. Aspinall, X. Ma, and M. Joyce, "An investigation of the digital discrimination of neutrons and γ rays with organic scintillation detectors using an artificial neural network," *Nuclear Instruments and Methods in Physics Research Section A: Accelerators, Spectrometers, Detectors and Associated Equipment*, vol. 607, no. 3, pp. 620–628, 2009.
[18] W. Zhang, W. Tongyu, B. Zheng, L. Shiping, Y. Zhang, and Y. Zejie, "A real-time neutron-gamma discriminator based on the support vector machine method for the time-of-flight neutron spectrometer," *Plasma Science and Technology*, vol. 20, no. 4, p. 045601, 2018.
[19] A. Hachem, A. Kanj, Y. Moline, G. Corre, C. Lynde and F. Carrel, "Neutron/gamma discrimination performance with plastic scintillator according to SNR, vertical resolution and sampling frequency," in *2022 IEEE Nuclear Science Symposium (NSS), Medical Imaging Conference (MIC) and Room Temperature Semiconductor Detector (RTSD) Conference*, "2022 forthcoming".
[20] C. Lynde, E. Montbarbon, M. Hamel, A. Grabowski, C. Frangville, G. H. Bertrand, G. Galli, F. Carrel, V. Schoepff, and Z. El Bitar, "Optimization of the charge comparison method for multiradiation field using various measurement systems," *IEEE Transactions on Nuclear Science*, vol. 67, no. 4, pp. 679–687, 2020.
[21] F. J. Harris, *Multirate signal processing for communication systems*. River Publishers, 2021.
[22] S. Butterworth *et al.*, "On the theory of filter amplifiers," *Wireless Engineer*, vol. 7, no. 6, pp. 536–541, 1930.
[23] J. Kaiser and R. Schafer, "On the use of the I0-sinh window for spectrum analysis," *IEEE Transactions on Acoustics, Speech, and Signal Processing*, vol. 28, no. 1, pp. 105–107, 1980.
[24] C. Kim, Y. Kim, M. Moon, and G. Cho, "Iterative Monte Carlo simulation with the Compton kinematics-based GEB in a plastic scintillation detector," *Nuclear Instruments and Methods in Physics Research Section A: Accelerators, Spectrometers, Detectors and Associated Equipment*, vol. 795, pp. 298–304, 2015.
[25] C. J. Werner, J. S. Bull, C. J. Solomon, F. B. Brown, G. W. McKinney, M. E. Rising, D. A. Dixon, R. L. Martz, H. G. Hughes, L. J. Cox, A. J. Zukaitis, J. C. Armstrong, R. A. Forster, and L. Casswell, "MCNP version 6.2 release notes," 2 2018. [Online]. Available: https://www.osti.gov/biblio/1419730
[26] P. Colangelo, O. Segal, A. Speicher, and M. Margala, "AutoML for multilayer perceptron and FPGA co-design," in *2020 IEEE 33rd International System-on-Chip Conference (SOCC)*. IEEE, 2020, pp. 265–266.
[27] A. Sanaullah, C. Yang, Y. Alexeev, K. Yoshii, and M. C. Herbordt, "Real-time data analysis for medical diagnosis using FPGA-accelerated neural networks," *BMC bioinformatics*, vol. 19, pp. 19–31, 2018.